Available online at www.sciencedirect.com
SCIENCE DIRECT
Catalysis Today 111 (2006) 403–411
CATALYSIS TODAY
www.elsevier.com/locate/cattod

# Ethylene dimerization over $NiSO_4$ supported on $Fe_2O_3$-promoted $ZrO_2$ catalyst

Jong Rack Sohn *, Jun Seob Lim

*Department of Applied Chemistry, Engineering College, Kyungpook National University, Taegu 702-701, Republic of Korea*

Available online 9 December 2005

**Abstract**

The $NiSO_4$ supported on $Fe_2O_3$-promoted $ZrO_2$ catalysts were prepared by the impregnation method. $Fe_2O_3$-promoted $ZrO_2$ was prepared by the coprecipitation method using a mixed aqueous solution of zirconium oxychloride and iron nitrate solution followed by adding an aqueous ammonia solution. No diffraction line of nickel sulfate was observed up to 20 wt.%, indicating good dispersion of nickel sulfate on the surface of $Fe_2O_3$–$ZrO_2$. The addition of nickel sulfate (or $Fe_2O_3$) to $ZrO_2$ shifted the phase transition of $ZrO_2$ (from amorphous to tetragonal) to higher temperatures because of the interaction between nickel sulfate (or $Fe_2O_3$) and $ZrO_2$. 15-$NiSO_4$/5-$Fe_2O_3$–$ZrO_2$ containing 15 wt.% $NiSO_4$ and 5 mol% $Fe_2O_3$, and calcined at 500 °C exhibited a maximum catalytic activity for ethylene dimerization. $NiSO_4$/$Fe_2O_3$–$ZrO_2$ catalysts was very effective for ethylene dimerization even at room temperature, but $Fe_2O_3$–$ZrO_2$ without $NiSO_4$ did not exhibit any catalytic activity at all. The catalytic activities were correlated with the acidity of catalysts measured by the ammonia chemisorption method. The addition of $Fe_2O_3$ up to 5 mol% enhanced the acidity, surface area, thermal property, and catalytic activities of catalysts gradually, due to the interaction between $Fe_2O_3$ and $ZrO_2$ and due to consequent formation of Fe–O–Zr bond.


*Keywords:* $Fe_2O_3$-promoted $NiSO_4$ catalyst; Phase transition of $ZrO_2$; Acidic properties; Ethylene dimerization

## 1. Introduction

The dimerization of alkenes is an important method for the production of higher olefins which find extensive application as industrial intermediate. A considerable number of papers have dealt with the problem of nickel-containing catalysts for ethylene dimerization [1–11]. One of the remarkable features of this catalyst system is its activity in relation to a series of *n*-olefins. In contrast to usual acid-type catalysts, nickel oxide on silica or silica–alumina shows a higher activity for a lower olefin dimerization, particularly for ethylene [1–6,12]. It has been suggested that the active site for dimerization is formed by an interaction of a low-valent nickel ion with an acid site [9,13]. It has been reported that the dimerization activities of such catalysts are related to the acidic properties of surface and low-valent nickel ions. In fact, nickel oxide, which is active for $C_2H_4$–$C_2D_4$ equilibration, acquires an activity for ethylene dimerization upon addition of nickel sulfate, which is known to be an acid [14]. A transition metal can also be supported on zeolite in the state of a cation or a finely dispersed metal. Transition metal ions like $Ni^+$ or $Pd^+$ can be active sites in catalytic reactions such as ethylene and propylene dimerization as well as acetylene cyclomerization [15–17].

The previous papers from this laboratory have shown that NiO–$TiO_2$ and NiO–$ZrO_2$ modified with sulfate or tungstate ions are very active for ethylene dimerization [6,18–20]. High catalytic activities in the reactions were attributed to the enhanced acidic properties of the modified catalysts, which originated from the inductive effect of S=O or W=O bonds of the complex formed by the interaction of oxides with sulfate or tungstate ions. However, catalytic functions have been improved by loading additional components. Sulfated zirconia incorporating Fe and Mn has been shown to be highly active for butane isomerization, catalyzing the reaction even at room temperature [21,22]. The promotion in activity of catalyst has been confirmed by several other research group [23–25]. Coelho et al. have discovered that the addition of Ni to sulfated zirconia causes an activity enhancement comparable to that

* Corresponding author. Tel.: +82 53 950 5585; fax: +82 53 950 6594.
*E-mail address:* jrsohn@knu.ac.kr (J.R. Sohn).

0920-5861/$ – see front matter © 2005 Elsevier B.V. All rights reserved.
doi:10.1016/j.cattod.2005.10.052

caused the addition of Fe and Mn [26]. It has been reported by several workers that the addition of platinum to zirconia modified by sulfate ions enhances catalytic activity in the skeletal isomerization of alkanes without deactivation when the reaction is carried out in the presence of hydrogen [27–29]. Recently, it has been found that a main group element Al can also promote the catalytic activity and stability of sulfated zirconia for *n*-butane isomerization [30–32].

Many metal sulfates generate fairly large amounts of acid sites of moderate or strong strength on their surfaces when they are calcined at 400–700 °C [33,34]. The acidic property of metal sulfate often gives high selectivity for diversified reactions such as hydration, polymerization, alkylation, cracking, and isomerization. However, structural and physicochemical properties of supported metal sulfates are considered to be in different states compared with bulk metal sulfates because of their interaction with supports [9,10,35]. Our previous work has shown that $NiSO_4$ supported on $ZrO_2$ is active for ethylene dimerization [36]. As an extension of the study on the ethylene dimerization, we prepared a new catalyst of $NiSO_4/Fe_2O_3$–$ZrO_2$ and the promoting effect of $Fe_2O_3$ on catalytic activity was studied.

## 2. Experimental

### 2.1. Catalyst preparation

The $Fe_2O_3$–$ZrO_2$ mixed oxide was prepared by a coprecipitation method using aqueous ammonia as the precipitation reagent. The coprecipitate of $Fe(OH)_3$–$Zr(OH)_4$ was obtained by adding aqueous ammonia slowly into a mixed aqueous solution of iron nitrate and zirconium oxychloride (Junsei Chemical Co.) at room temperature with stirring until the pH of the mother liquor reached about 8. Catalysts containing various nickel sulfate contents were prepared by the impregnation of $Fe(OH)_3$–$Zr(OH)_4$ powder with an aqueous solution of $NiSO_4$, followed by calcining at different temperatures for 1.5 h in air. This series of catalysts is denoted by the mole percentage of $Fe_2O_3$ and the weight percentage of nickel sulfate. For example, 15-$NiSO_4$/5-$Fe_2O_3$–$ZrO_2$ indicates the catalyst containing 5 mol% of $Fe_2O_3$ and 15 wt.% of $NiSO_4$.

### 2.2. Procedure

FT-IR spectra were obtained in a heatable gas cell at room temperature using a Mattson Model GL6030E spectrophotometer. The self-supporting catalyst wafers contained about 10 mg $cm^{-2}$. Prior to obtaining the spectra, we heated each sample under vacuum at 25–500 °C for 1 h. Catalysts were checked in order to determine the structure of the prepared catalysts by means of a Philips X'pert-APD X-ray diffractometer, employing Ni-filtered Cu Kα radiation. DSC measurements were performed by a PL-STA model 1500H apparatus in air; the heating rate was 5 °C/min. For each experiment 10–15 mg of sample was used.

The specific surface area was determined by applying the BET method to the adsorption of $N_2$ at −196 °C. Chemisorption of ammonia was also employed as a measure of the acidity of catalysts. The amount of chemisorption was determined based on the irreversible adsorption of ammonia [20,37,38].

The catalytic activity for ethylene dimerization was determined at 20 °C using a conventional static system following the pressure change from an initial pressure of 290 Torr. A fresh catalyst sample of 0.2 g was used for every run and the catalytic activity was calculated as the initial rate calculated from the initial activity slope. Reaction products were analyzed by gas chromatography with a VZ-7 column at room temperature.

## 3. Results and discussion

### 3.1. Infrared spectra

The infrared spectra of 15-$NiSO_4$/5-$Fe_2O_3$–$ZrO_2$ (KBr disc) calcined at different temperatures (400–800 °C) are given in Fig. 1. 15-$NiSO_4$/5-$Fe_2O_3$–$ZrO_2$ calcined up to 700 °C showed infrared absorption bands at 1204, 1133, 1098 and 987 $cm^{-1}$, which are assigned to bidentate sulfate ions coordinated to the metal such as $Zr^{4+}$ or $Fe^{3+}$ [39,40]. The band at 1625 $cm^{-1}$ is assigned to the deformation vibration mode of the adsorbed water. For 15-$NiSO_4$/5-$Fe_2O_3$–$ZrO_2$ calcined at 700 °C, the band intensities of sulfate ion decreased because of the partial decomposition of sulfate ion. However, for the sample calcined at 800 °C, infrared bands by the sulfate ion disappeared completely due to the decomposition of sulfate ion.

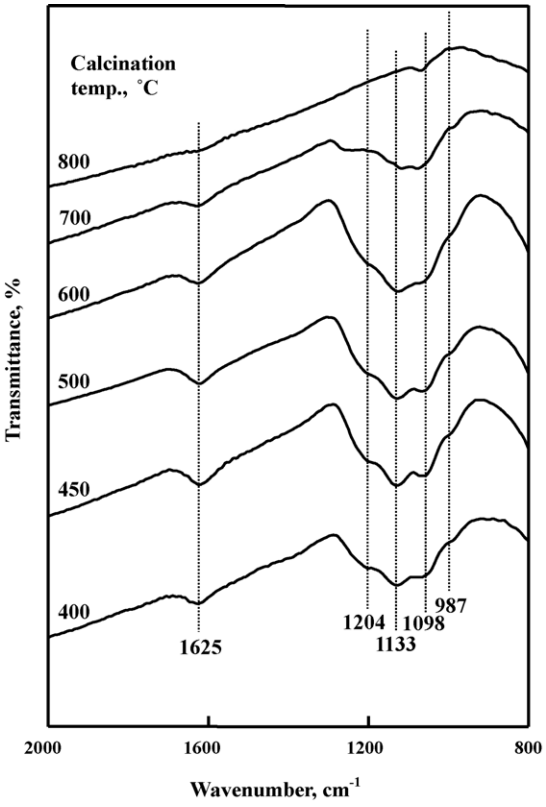


Fig. 1. Infrared spectra of 15-$NiSO_4$/5-$Fe_2O_3$–$ZrO_2$ calcined at different temperatures for 1.5 h.

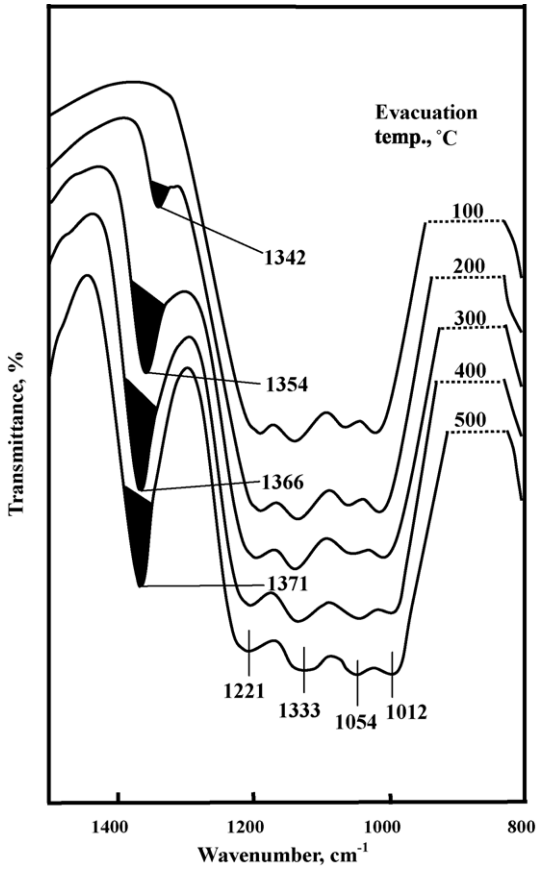


Fig. 2. Infrared spectra of 15-$NiSO_4$/5-$Fe_2O_3$–$ZrO_2$ evacuated at different temperatures for 1 h.

In general, for the metal oxides modified with sulfate ions followed by evacuation above 400 °C, a strong band [41,42] assigned to S=O stretching frequency is observed at 1390–1360 $cm^{-1}$. In a separate experiment, the infrared spectrum of self-supported 15-$NiSO_4$/5-$Fe_2O_3$–$ZrO_2$ after evacuation at 100–500 °C for 1 h was examined. As shown in Fig. 2, an intense band at 1342–1371 $cm^{-1}$ accompanied by four broad but split bands at 1221, 1133, 1054 and 1012 $cm^{-1}$, indicating the presence of different adsorbed species depending on the treatment conditions of the sulfated sample [43]. At 100 °C an asymmetric stretching band of S=O bonds was not observed because water molecules are adsorbed on the surface of 15-$NiSO_4$/5-$Fe_2O_3$–$ZrO_2$ [30,44]. At 200 °C the S=O stretching band appeared at 1342 $cm^{-1}$. The band intensity increased with the evacuation temperature and the position of band shifted to a higher wavenumber. That is, the higher the evacuation temperature, the larger was the shift of the asymmetric stretching frequency of the S=O bonds. It is likely that the surface sulfur complexes formed by the interaction of oxides with sulfate ions in highly active catalysts have a strong tendency to reduce their bond order by the adsorption of basic molecules such as $H_2O$ [30,44]. When the 15-$NiSO_4$/5-$Fe_2O_3$–$ZrO_2$ sample evacuated at 500 °C was exposed to air at 25 °C, the drastic shift of the IR band from 1371 $cm^{-1}$ to lower wavenumber (not shown due to the overlaps with skeletal vibration band of $Fe_2O_3$ and $ZrO_2$) occurred because of the adsorption of water, resulting in the appearance of adsorbed water band at 1625 $cm^{-1}$. Consequently, as shown in Fig. 2, an asymmetric stretching band of S=O bonds for the sample evacuated at a lower temperature appears at a lower frequency compared with that for the sample evacuated at higher temperature because the adsorbed water reduces the bond order of S=O from a highly covalent double-bond character to a lesser double-bond character.

### 3.2. Crystalline structures of catalysts

The crystalline structures of 15-$NiSO_4$/5-$Fe_2O_3$–$ZrO_2$ calcined in air at different temperatures for 1.5 h were checked by X-ray diffraction. In the case of supported nickel sulfate catalysts, the crystalline structures of the samples were different from the structure of the $ZrO_2$, support. The 15-$NiSO_4$/5-$Fe_2O_3$–$ZrO_2$ materials calcined at different temperatures, as shown in Fig. 3, are amorphous up to 600 °C. In other words, the transition temperature from amorphous to tetragonal phase was higher by 350 °C than that of pure $ZrO_2$ [36]. X-ray diffraction data indicated only the tetragonal phase of $ZrO_2$ at 700–800 °C, without detection of orthorhombic $NiSO_4$ phase. It is assumed that the interaction between $NiSO_4$ (or $Fe_2O_3$) and $ZrO_2$ hinders the phase transition of $ZrO_2$ from amorphous to tetragonal [30]. For the above $Fe_2O_3$-promoted catalysts, there

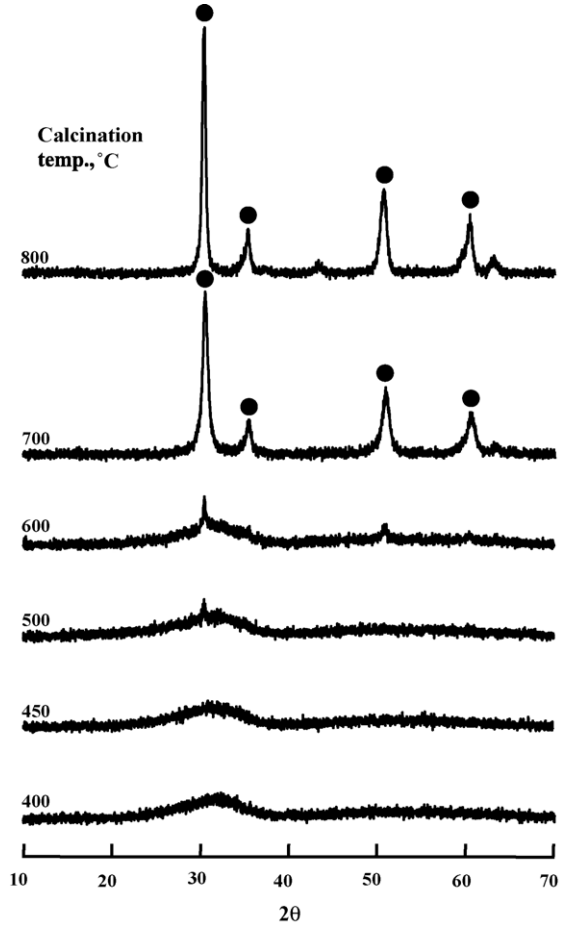


Fig. 3. X-ray diffraction patterns of 15-$NiSO_4$/5-$Fe_2O_3$–$ZrO_2$ calcined at different temperatures for 1.5 h: (●) tetragonal phase of $ZrO_2$.

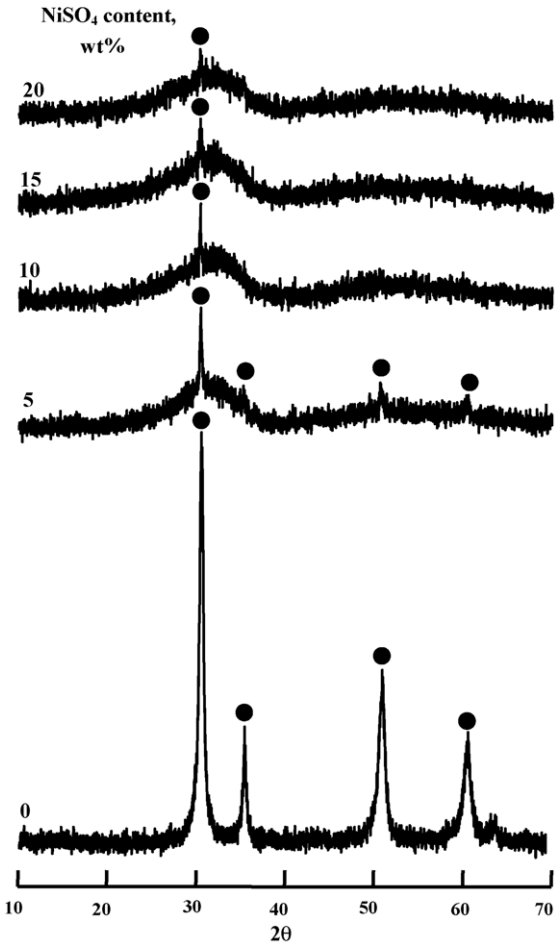


Fig. 4. X-ray diffraction patterns of $NiSO_4$/5-$Fe_2O_3$–$ZrO_2$ containing different $NiSO_4$ contents and calcined at 500 °C for 1.5 h: (●) tetragonal phase of $ZrO_2$.

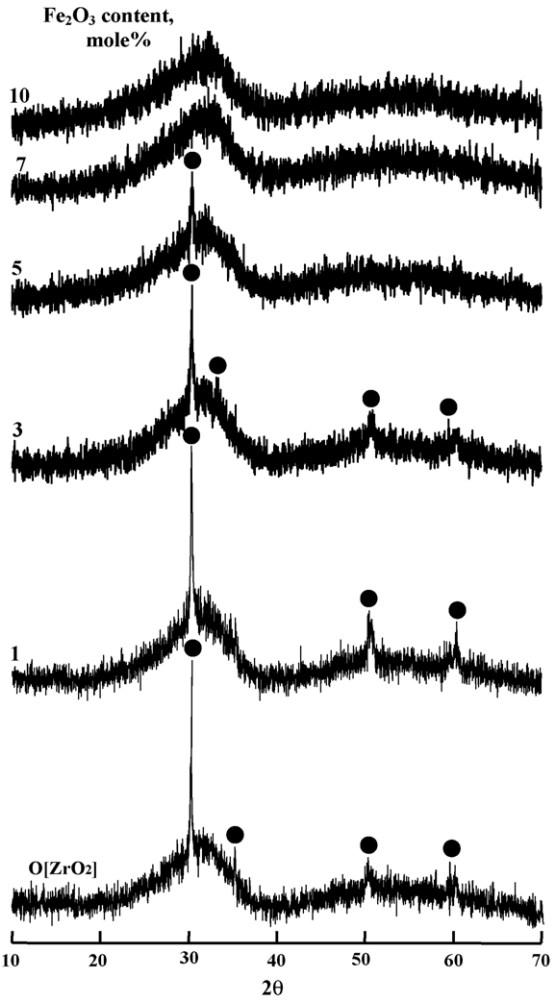


Fig. 5. X-ray diffraction patterns of 15-$NiSO_4$/$Fe_2O_3$–$ZrO_2$ containing different $Fe_2O_3$ contents and calcined at 500 °C for 1.5 h: (●) tetragonal phase of $ZrO_2$.

are no characteristic peaks of $Fe_2O_3$ in the patterns, implying that $Fe_2O_3$ is sufficiently homogeneously mixed with zirconia.

The XRD patterns of $NiSO_4$/5-$Fe_2O_3$–$ZrO_2$ containing different nickel sulfate contents and calcined at 500 °C for 1.5 h are shown in Fig. 4. XRD data indicated only tiny amount of tetragonal phase of $ZrO_2$ at the region of 5–20 wt.% of nickel sulfate, indicating good dispersion of $NiSO_4$ on the surface of 5-$Fe_2O_3$–$ZrO_2$. However, the higher the content of $NiSO_4$, the lower is the amount of tetragonal $ZrO_2$ phase as in the case of $Fe_2O_3$ addition described below, because the interaction between nickel sulfate and $ZrO_2$ hinders the phase transition of $ZrO_2$ from amorphous to tetragonal in proportion to the nickel sulfate content [40].

The XRD patterns of 15-$NiSO_4$/$Fe_2O_3$–$ZrO_2$ containing different $Fe_2O_3$ contents and calcined at 500 °C for 1.5 h are shown in Fig. 5. XRD data indicated only the tetragonal phase of $ZrO_2$ at the region of 0–5 mol% of $Fe_2O_3$. However, the higher the content of $Fe_2O_3$, the lower is the amount of tetragonal $ZrO_2$ phase as in the case of $NiSO_4$ addition, showing only amorphous phase for the sample above 5 mol% $Fe_2O_3$, because the interaction between $Fe_2O_3$ and $ZrO_2$ hinders the phase transition of $ZrO_2$ from amorphous to tetragonal in proportion to the $Fe_2O_3$ content [40]. In this case, no crystalline phase of $Fe_2O_3$ was observed on the X-ray diffraction patterns.

### 3.3. Thermal analysis

The X-ray diffraction patterns in Figs. 3–5 clearly show that the structure of $NiSO_4$/$Fe_2O_3$–$ZrO_2$ is different depending on the calcined temperature. To examine the thermal properties of precursors of $NiSO_4$/$Fe_2O_3$–$ZrO_2$ samples more clearly, we completed their thermal analysis; the results are illustrated in Figs. 6 and 7. For pure $ZrO_2$, the DSC curve shows a broad endothermic peak below 200 °C due to water elimination, and a sharp exothermic peak at 418 °C due to the $ZrO_2$ crystallization [40]. However, it is of interest to see the influence of $Fe_2O_3$ on the crystallization of $ZrO_2$ from amorphous to tetragonal phase. As Fig. 6 shows, the exothermic peak due to the crystallization appears at 418 °C for pure $ZrO_2$, while for $Fe_2O_3$–$ZrO_2$ samples it is shifted to higher temperatures due to the interaction between $Fe_2O_3$ and $ZrO_2$. The shift increases with increasing $Fe_2O_3$ content. Consequently, the exothermic peaks appear at 446 °C for 1-$Fe_2O_3$–$ZrO_2$, 465 °C for 3-$Fe_2O_3$–$ZrO_2$, 485 °C for 5-$Fe_2O_3$–$ZrO_2$, 501 °C for 7-$Fe_2O_3$–$ZrO_2$, 529 °C for 10-$Fe_2O_3$–$ZrO_2$, and 558 °C for 15-$Fe_2O_3$–$ZrO_2$.

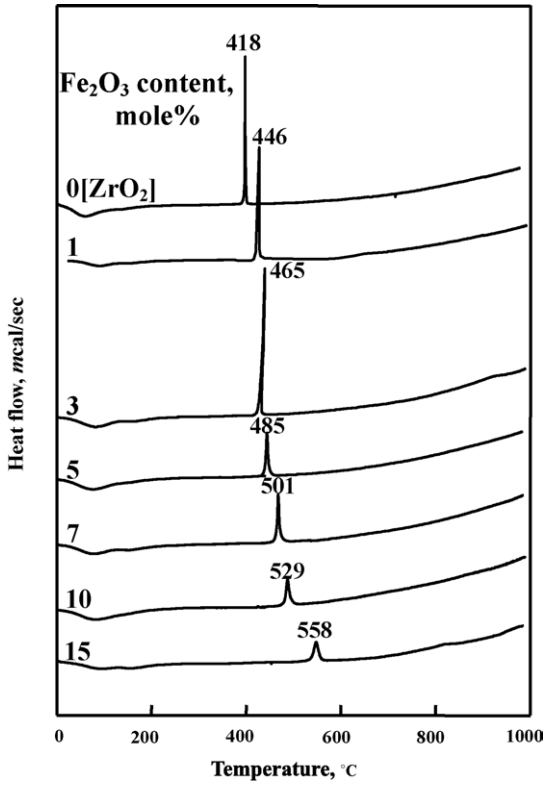


Fig. 6. DSC curves of $Fe_2O_3$–$ZrO_2$ precursors containing different $Fe_2O_3$ contents.

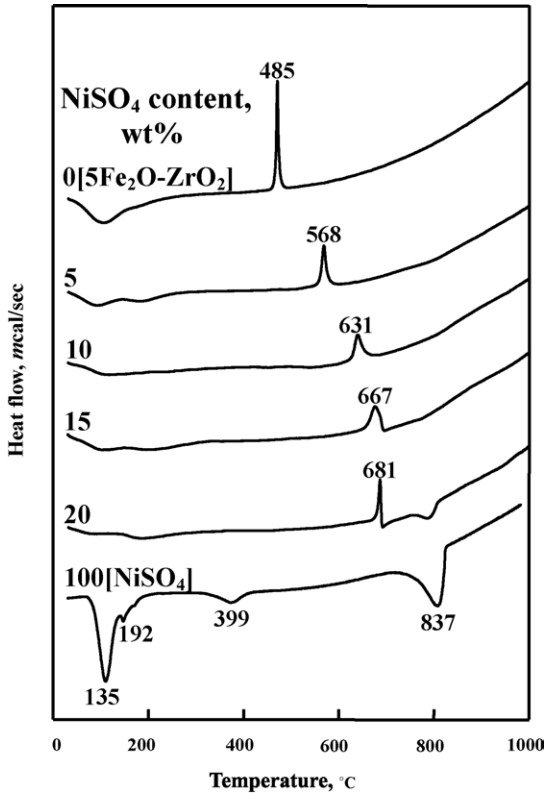


Fig. 7. DSC curves of $NiSO_4$/5-$Fe_2O_3$–$ZrO_2$ precursors containing different $NiSO_4$ contents.

However, for $NiSO_4$/5-$Fe_2O_3$–$ZrO_2$ samples containing different $NiSO_4$ contents, the DSC patterns are somewhat different from that of $Fe_2O_3$–$ZrO_2$. As shown in Fig. 7, the exothermic peak for $NiSO_4$/5-$Fe_2O_3$–$ZrO_2$ due to the crystallization of $ZrO_2$ is shifted to higher temperatures compared with that for 5-$Fe_2O_3$–$ZrO_2$ without $NiSO_4$, indicating that there is an interaction between $NiSO_4$ and $ZrO_2$ in addition to the interaction between $Fe_2O_3$ and $ZrO_2$. For pure $NiSO_4{\cdot}6H_2O$, the DSC curve shows three endothermic peaks below 400 °C due to water elimination, indicating that the dehydration of $NiSO_4{\cdot}6H_2O$ occurs in three steps. The endothermic peak around 837 °C is due to the evolution of $SO_3$ decomposed from nickel sulfate [30,44]. Decomposition of nickel sulfate is known to begin at 700 °C [45].

### 3.4. Surface properties

#### 3.4.1. Specific surface area and acidity

The specific surface areas of samples containing different $NiSO_4$ contents and calcined at 500 °C for 1.5 h are listed in Table 1. The presence of nickel sulfate and $Fe_2O_3$ influences the surface area in comparison with that of the pure $ZrO_2$. Specific surface areas of $NiSO_4$/5-$Fe_2O_3$–$ZrO_2$ samples are larger than that of 5-$Fe_2O_3$–$ZrO_2$ calcined at the same temperature, showing that surface area increases gradually with increasing nickel sulfate loading up to 15 wt.%. It seems likely that the interactions between nickel sulfate (or $Fe_2O_3$) and $ZrO_2$ prevent catalysts from crystallizing [46]. The decrease of surface area for $NiSO_4$/5-$Fe_2O_3$–$ZrO_2$ samples containing $NiSO_4$ above 15 wt.% is due to the blocking of $ZrO_2$ pores by the increased $NiSO_4$ loading. The acidity of catalysts calcined at 500 °C, as determined by the amount of $NH_3$ irreversibly adsorbed at 230 °C [20,37,38], is also listed in Table 1. The variation of acidity runs parallel to the change of surface area. The acidity increases with increasing nickel sulfate content up to 15 wt.% of $NiSO_4$. The acidity is correlated with the catalytic activity for the ethylene dimerization discussed below.

#### 3.4.2. Effect of $Fe_2O_3$ addition on surface properties

We examined the effect of $Fe_2O_3$ addition on the surface area and acidity of $NiSO_4$/$Fe_2O_3$–$ZrO_2$ samples. The specific surface areas and acidity of 15-$NiSO_4$/$Fe_2O_3$–$ZrO_2$ catalysts containing different $Fe_2O_3$ contents and calcined at 500 °C are listed in Table 2. Both surface area and acidity increased with increasing $Fe_2O_3$ content up to 5 mol%, indicating the

Table 1
Surface area and acidity of $NiSO_4$/5-$Fe_2O_3$–$ZrO_2$ catalysts containing different $NiSO_4$ contents and calcined at 500 °C for 1.5 h

| $NiSO_4$ content (wt.%) | Surface area ($m^2$/g) | Acidity (μmol/g) |
|---|---|---|
| 0 | 81 | 73 |
| 5 | 109 | 113 |
| 10 | 123 | 191 |
| 15 | 168 | 227 |
| 20 | 130 | 186 |
| 100 | 30 | 79 |

Table 2
Surface area and acidity of 15-$NiSO_4$/5-$Fe_2O_3$–$ZrO_2$ catalysts containing different $Fe_2O_3$ contents and calcined at 500 °C for 1.5 h

| $Fe_2O_3$ content (mol%) | Surface area ($m^2$/g) | Acidity (μmol/g) |
|---|---|---|
| 0 | 86 | 141 |
| 1 | 131 | 168 |
| 3 | 147 | 186 |
| 5 | 168 | 227 |
| 7 | 156 | 171 |
| 10 | 143 | 149 |

promoting effect of $Fe_2O_3$ on the catalytic activities for ethylene dimerization described later.

Infrared spectroscopic studies of ammonia adsorbed on solid surfaces have made it possible to distinguish between Brönsted and Lewis acid sites [44,47,48]. Fig. 8 shows the infrared spectra of ammonia adsorbed on 15-$NiSO_4$/5-$Fe_2O_3$–$ZrO_2$ samples evacuated at 500 °C for 1 h. For 15-$NiSO_4$/5-$Fe_2O_3$–$ZrO_2$ the band at 1432 $cm^{-1}$ is the characteristic peak of ammonium ion, which is formed on the Brönsted acid sites and the absorption peak at 1612 $cm^{-1}$ is contributed by ammonia coordinately bonded to Lewis acid sites [44,47,48], indicating the presence of both Brönsted and Lewis acid sites on the surface of 15-$NiSO_4$/5-$Fe_2O_3$–$ZrO_2$ samples. Other samples having different nickel sulfate contents also showed the presence of both Lewis and Brönsted acids. As Fig. 8(a) shows,

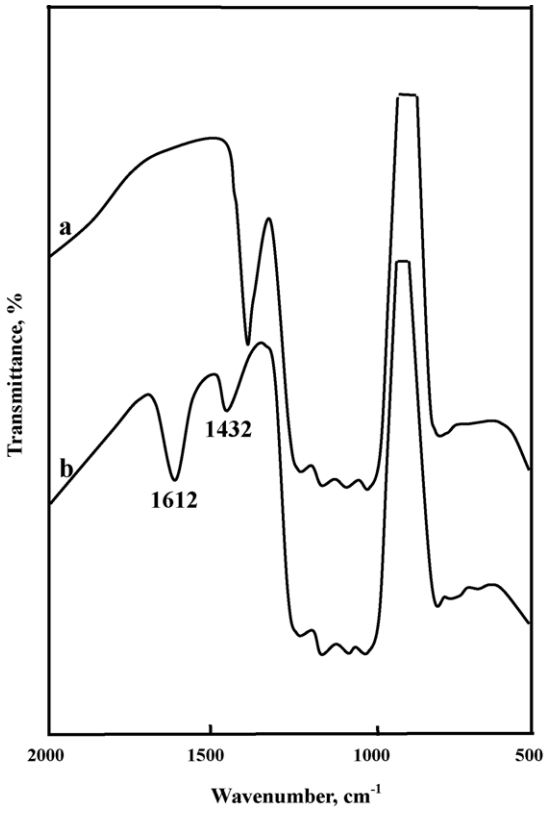


Fig. 8. Infrared spectra of $NH_3$ adsorbed on 15-$NiSO_4$/5-$Fe_2O_3$–$ZrO_2$: (a) background of 15-$NiSO_4$/5-$Fe_2O_3$–$ZrO_2$ after evacuation at 500 °C for 1 h, (b) $NH_3$ adsorbed on (a), where gas was evacuated at 230 °C for 1 h.

the intense band at 1371 $cm^{-1}$ after evacuation at 500 °C is assigned to the asymmetric stretching vibration of S=O bonds having a high double-bond nature [42,44]. However, the drastic shift of the infrared band from 1371 $cm^{-1}$ to a lower wavenumber (not shown due to the overlaps of skeletal vibration bands of $Fe_2O_3$–$ZrO_2$) after ammonia adsorption (Fig. 8(b)) indicates a strong interaction between an adsorbed ammonia molecule and the surface complex. Namely, the surface sulfur compound in the highly acidic catalysts has a strong tendency to reduce the bond order of S=O from a highly covalent double-bond character to a lesser double-bond character when a basic ammonia molecule is adsorbed on the catalysts [42,44].

Acids stronger than $H_0 \leq -11.93$, which corresponds to the acid strength of 100% $H_2SO_4$, are superacids [33,42,49,50]. The strong ability of the sulfur complex to accommodate electrons from a basic molecule such as ammonia is a driving force to generate superacidic properties [33,42,51]. $NiSO_4$/$Fe_2O_3$–$ZrO_2$ samples after evacuation at 500 °C for 1 h was also examined by a color change method, using Hammett indicator in sulfuryl chloride [37,52]. The samples were estimated to have $H_0 \leq -14.5$, indicating the formation of superacidic sites. Consequently, $NiSO_4$/$Fe_2O_3$–$ZrO_2$ catalysts would be solid superacids, in analogy with the case of metal oxides modified with a sulfate group [20,42,48,53]. This superacidic property is attributable to the double-bond nature of the S=O in the complex formed by the interaction between $NiSO_4$ and $Fe_2O_3$–$ZrO_2$ [9,33,42,53]. In other words, the acid strength of $NiSO_4$/$Fe_2O_3$–$ZrO_2$ becomes stronger by the inductive effect of S=O in the complex.

### 3.5. Catalytic activities for ethylene dimerization

#### 3.5.1. Ethylene dimerization

$NiSO_4$/$Fe_2O_3$–$ZrO_2$ catalysts were tested for their effectiveness in ethylene dimerization. Over 15-$NiSO_4$/$ZrO_2$, 15-$NiSO_4$/3-$Fe_2O_3$–$ZrO_2$, and 15-$NiSO_4$/5-$Fe_2O_3$–$ZrO_2$, ethylene was continuously consumed, as shown by the results presented in Fig. 9, where catalysts were evacuated at 500 °C for 1 h. Over three catalysts, ethylene was selectively dimerized to *n*-butenes. In the composition of *n*-butenes analyzed by gas chromatography, 1-butene was found to predominate exclusively at the initial reaction time, as compared with *cis*-butene and *trans*-butene. This is because the initial product of ethylene dimerization is 1-butene [4,9,48]. Therefore, the initially produced 1-butene is also isomerized to 2-butene during the reaction time [18–20,44]. As shown in Fig. 9, the catalytic activities of 15-$NiSO_4$/3-$Fe_2O_3$–$ZrO_2$ and 15-$NiSO_4$/5-$Fe_2O_3$–$ZrO_2$ are higher than that of 15-$NiSO_4$/$ZrO_2$ without $Fe_2O_3$, showing a clear $Fe_2O_3$-promoted effect on catalytic activity for ethylene dimerization discussed below.

The catalytic activities of 15-$NiSO_4$/5-$Fe_2O_3$–$ZrO_2$ were tested as a function of calcination temperature (not shown in the figure). The activities increased with the calcination temperature, reaching a maximum at 500 °C, after which the activities

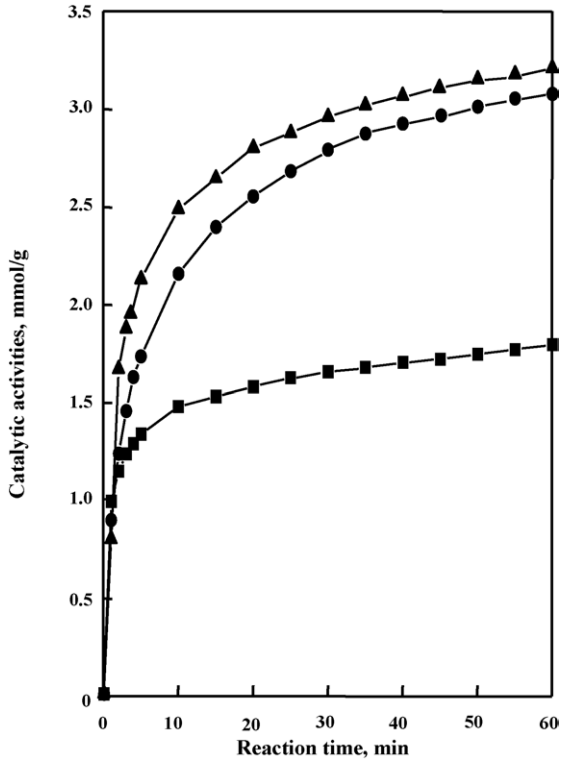


Fig. 9. Time–course of ethylene dimerization over catalysts evacuated at 500 °C for 1 h: (▲) 15-$NiSO_4$/5-$Fe_2O_3$–$ZrO_2$; (●) 15-$NiSO_4$/3-$Fe_2O_3$–$ZrO_2$; (■) 15-$NiSO_4$/$ZrO_2$.

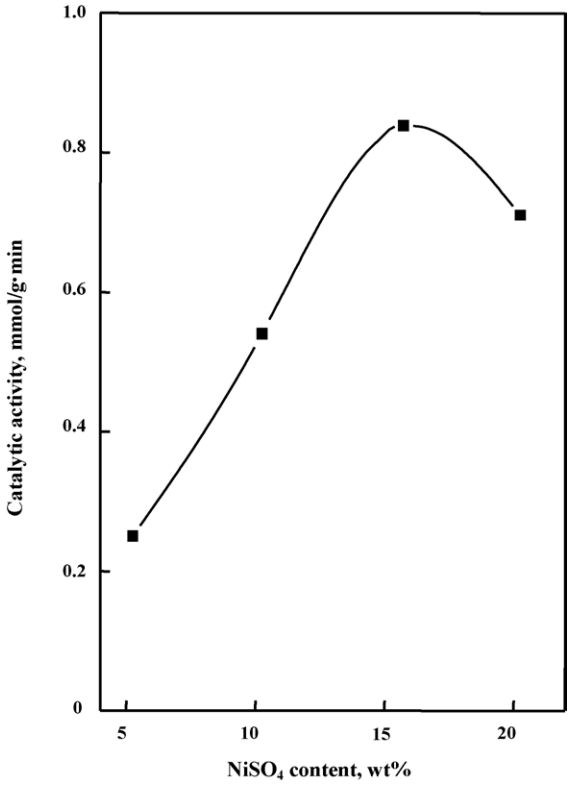


Fig. 10. Catalytic activity of $NiSO_4$/5-$Fe_2O_3$–$ZrO_2$ for ethylene dimerization as a function of $NiSO_4$ content.

decreased. The decrease of catalytic activity after calcination above 500 °C can be probably attributed to the fact that the surface area and acidity above 500 °C decrease with the calcination temperature. Thus, hereafter, emphasis is placed only on the $NiSO_4$/$Fe_2O_3$–$ZrO_2$ samples calcined at 500 °C.

### 3.5.2. *Catalytic activity as a function of $NiSO_4$ content*

The catalytic activity of $NiSO_4$/5-$Fe_2O_3$–$ZrO_2$ containing different $NiSO_4$ contents was examined; the results are shown as a function of $NiSO_4$ content in Fig. 10. Catalysts were evacuated at 500 °C for 1 h before each reaction. The catalytic activity gives a maximum at 15 wt.% of $NiSO_4$. This seems to be correlated to the specific surface area and to the acidity of catalysts. The acidity of $NiSO_4$/5-$Fe_2O_3$–$ZrO_2$ calcined at 500 °C was determined by the amount of $NH_3$ irreversibly adsorbed at 230 °C [20,37,38]. As listed in Table 1, the BET surface area attained a maximum extent when the $NiSO_4$ content in the catalyst was 15 wt.% and then showed a gradual decrease with increasing $NiSO_4$ content. In view of Table 1 and Fig. 10, the higher the acidity, the higher the catalytic activity. Good correlations have been found in many cases between the acidity and the catalytic activities of solid acids. For example, the rates of both the catalytic decomposition of cumene and the polymerization of propylene over $SiO_2$–$Al_2O_3$ catalysts were found to increase with increasing acid amount at strength $H_0 \leq +3.3$ [54]. The catalytic activity of nickel-containing catalysts in ethylene dimerization as well as in butene isomerization is closely correlated with the acidity of the catalyst [4,9,10].

### 3.5.3. *Promoting effect of $Fe_2O_3$ on catalytic activity*

The catalytic activity of 15-$NiSO_4$/$Fe_2O_3$–$ZrO_2$ as a function of $Fe_2O_3$ content for the reaction of ethylene dimerization was examined. Here the catalysts were evacuated at 500 °C for 1 h before reaction; the results are shown in Fig. 11. The catalytic activity increased with increasing the $Fe_2O_3$ content, reaching a maximum at 5 mol%.

Considering the experimental results of Table 2 and Fig. 11, we think that the catalytic activities for ethylene dimerization are closely related to the changes of surface area and the acidity of catalysts. As listed in Table 2, the total acid sites of 15-$NiSO_4$/5-$Fe_2O_3$–$ZrO_2$ and 15-$NiSO_4$/$ZrO_2$ are 227 and 141 μmol/g, respectively, showing that the number of acid sites for the catalyst promoted with $Fe_2O_3$ is greater than that for non-promoted catalyst. This is consistent with the results reported by Hua et al. [30] over $Fe_2O_3$-promoted $SO_4^{2-}$/$ZrO_2$. $Fe_2O_3$-promoted catalysts could be related to a strong interaction between $Fe_2O_3$ and $ZrO_2$. Since the promoting effect of $Fe_2O_3$ is related to an increase in number of surface acidic sites, it would be of interest to examine various factors influencing the enhancement of these surface acidic sites.

Xia et al. [55] proposed that $Fe_2O_3$ incorporation in $ZrO_2$ matrix brought about an increase of the positive partial charge on the Zr cations as a result of the formation of Zr–O–Fe bonds which helped to stabilize the sulfate species at the oxide surface. The formation of Fe–O–Zr bond on the surface of the $Fe_2O_3$-promoted catalysts is probably the cause for the increase in strong acidic sites. According to the principle of electronegativity equalization proposed by Sanderson [56], since

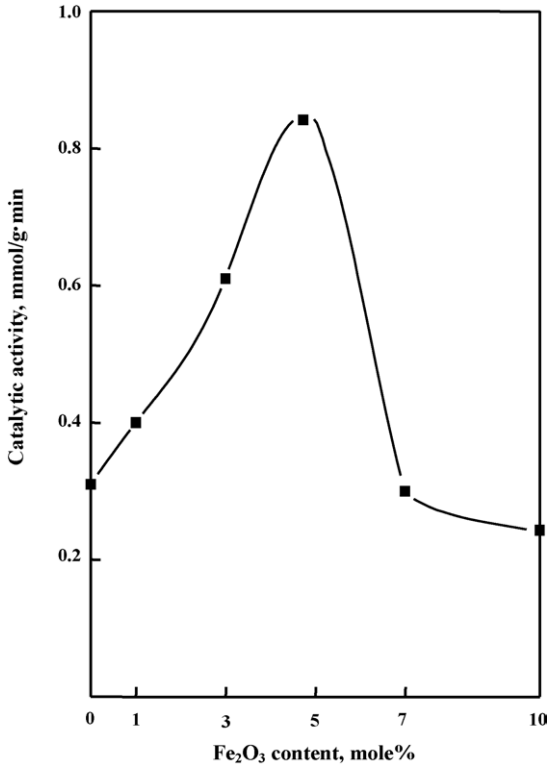


Fig. 11. Catalytic activity of 15-$NiSO_4/Fe_2O_3$–$ZrO_2$ for ethylene dimerization as a function of $Fe_2O_3$ content.

the electronegativity of $Fe^{3+}$ is larger than that of $Zr^{4+}$, the positive charge on Zr atom is increased as a result of the formation of Fe–O–Zr bond, which generates stronger acidity on these sites [30]. At the same time, the stronger Fe–O–Zr bond formed by the charge transfer from Zr atom to neighboring Fe atom results in an increase in the thermal stability of the surface sulfate species and consequently the acidity of $Fe_2O_3$-promoted catalyst is increased. In fact, to examine the thermal stability of the surface sulfate species DSC measurements were carried out. The endothermic peak due to the evolution of $SO_3$ decomposed from sulfate species bonded to the surface of $ZrO_2$ appeared at 730 °C [34], while that from sulfate species bonded to the surface of $Fe_2O_3$-promoted $ZrO_2$ appeared at 764 °C. Such a temperature difference has been attributed to the stabilizing effect of the $Fe_2O_3$ promoter on the sulfate species. Namely, the charge transfer from Zr atoms to the neighboring Fe atoms strengthens the Fe–O bond between Fe and the surface sulfate species. The stronger Fe–O bond leads to an increase in the thermal stability of the surface sulfate species and consequently the acidity of the catalysts is increased. A similar result was related by Gao et al. [57] to strong acid sites with differential heat of ammonia adsorption above 140 kJ $mol^{-1}$.

## 4. Conclusions

A series of catalysts, $NiSO_4/Fe_2O_3$–$ZrO_2$, were prepared by the impregnation method using an aqueous solution of nickel sulfate. The addition of nickel sulfate (or $Fe_2O_3$) to $ZrO_2$ shifted the phase transition of $ZrO_2$ (from amorphous to tetragonal) to higher temperatures because of the interaction between nickel sulfate (or $Fe_2O_3$) and $ZrO_2$. 15-$NiSO_4/Fe_2O_3$–$ZrO_2$ containing 15 wt.% $NiSO_4$ and 5 mol% $Fe_2O_3$, and calcined at 500 °C, exhibited maximum catalytic activities for ethylene dimerization. $NiSO_4/Fe_2O_3$–$ZrO_2$ catalysts was very effective for ethylene dimerization even at room temperature, but $Fe_2O_3$–$ZrO_2$ without $NiSO_4$ did not exhibit any catalytic activity at all. The catalytic activity was correlated with the acidity of catalysts measured by the ammonia chemisorption method. The addition of $Fe_2O_3$ up to 5 mol% enhanced the acidity, surface area, thermal properties, and catalytic activities of $NiSO_4/Fe_2O_3$–$ZrO_2$ gradually, due to the interaction between $Fe_2O_3$ and $ZrO_2$ and due to consequent formation of Fe–O–Zr bond.

## Acknowledgements

This work was supported by grant No. R05-2003-000-100740-0 from the Basic Research Program of the Korea Science and Engineering Foundation. We wish to thank Korea Basic Science Institute (Daegu Branch) for the use of their X-ray diffractometer.

## References

[1] Y.I. Pae, S.H. Lee, J.R. Sohn, Catal. Lett. 99 (2005) 241.
[2] F. Bernardi, A. Bottoni, I. Rossi, J. Am. Chem. Soc. 120 (1998) 7770.
[3] J.R. Sohn, A. Ozaki, J. Catal. 59 (1979) 303.
[4] J.R. Sohn, A. Ozaki, J. Catal. 61 (1980) 291.
[5] G. Wendt, E. Fritsch, R. Schöllner, H.Z. Siegel, Anorg. Allg. Chem. 467 (1980) 51.
[6] J.R. Sohn, D.C. Shin, J. Catal. 160 (1996) 314.
[7] G.F. Berndt, S.J. Thomson, G.J. Webb, J. Chem. Soc., Faraday Trans. 1 79 (1983) 195.
[8] T.V. Herwijnen, H.V. Doesburg, D.V. Jong, J. Catal. 28 (1973) 391.
[9] J.R. Sohn, W.C. Park, H.W. Kim, J. Catal. 209 (2002) 69.
[10] J.R. Sohn, W.C. Park, Bull. Korean Chem. Soc. 21 (2000) 1063.
[11] K. Urabe, M. Koga, Y. Izumi, J. Chem. Soc., Chem. Commun. (1989) 807.
[12] G. Wendt, D. Hentschel, J. Finster, R. Schöllner, J. Chem. Soc., Faraday Trans. 1 79 (1983) 2013.
[13] K. Kimura, A. Ozaki, J. Catal. 3 (1964) 395.
[14] K. Maruya, A. Ozaki, Bull. Chem. Soc. Jpn. 46 (1973) 351.
[15] M. Hartmann, A. Pöppl, L. Kevan, J. Phys. Chem. 100 (1996) 9906.
[16] I.V. Elev, B.N. Shelimov, V.B. Kazansky, J. Catal. 89 (1984) 470.
[17] H. Choo, L. Kevan, J. Phys. Chem. B 105 (2001) 6353.
[18] J.R. Sohn, H.J. Kim, J. Catal. 101 (1986) 428.
[19] J.R. Sohn, S.Y. Lee, Appl. Catal. A: Gen. 164 (1997) 127.
[20] J.R. Sohn, H.W. Kim, M.Y. Park, E.H. Park, J.T. Kim, S.E. Park, Appl. Catal. 128 (1995) 127.
[21] C.Y. Hsu, C.R. Heimbuch, C.T. Armes, B.C. Gates, J. Chem. Soc., Chem. Commun. (1992) 1645.
[22] T.K. Cheung, B.C. Gates, J. Catal. 168 (1997) 522.
[23] V. Adeeva, H.W. de Haan, J. Janchen, G.D. Lei, V. Schunemann, L.J.M. van de Ven, W.M.H. Sachtler, R.A. van Santen, J. Catal. 151 (1995) 364.
[24] K.T. Wan, C.B. Khouw, M.E. Davis, J. Catal. 158 (1996) 311.
[25] X. Song, K.R. Reddy, A. Sayari, J. Catal. 161 (1996) 206.
[26] M.A. Coelho, D.E. Resasco, E.C. Sikabwe, R.L. White, Catal. Lett. 32 (1995) 253.
[27] T. Hosoi, T. Shimadzu, S. Ito, S. Baba, H. Takaoka, T. Imai, N. Yokoyama, Prepr. Symp. Div. Petr. Chem., American Chemical Society, Los Angeles, CA, 1988, p. 562.
[28] K. Ebitani, J. Konishi, H. Hattori, J. Catal. 130 (1991) 257.
[29] M. Signoretto, F. Pinna, G. Strukul, P. Chies, G. Cerrato, S.D. Ciero, C. Morterra, J. Catal. 167 (1997) 522.

[30] W. Hua, Y. Xia, Y. Yue, Z. Gao, J. Catal. 196 (2000) 104.
[31] J.A. Moreno, G. Poncelet, J. Catal. 203 (2001) 153.
[32] J.R. Sohn, E.S. Cho, Appl. Catal. A: Gen. 282 (2005) 147.
[33] K. Tanabe, M. Misono, Y. Ono, H. Hattori, New Solid Acids and Bases, Kodansha/Elsevier, Tokyo, 1989, p. 185.
[34] K. Arata, M. Hino, N. Yamagata, Bull. Chem. Soc. Jpn. 63 (1990) 244.
[35] J.R. Sohn, E.H. Park, J. Ind. Eng. Chem. 4 (1998) 197.
[36] J.R. Sohn, W.C. Park, Appl. Catal. A: Gen. 230 (2002) 11.
[37] J.R. Sohn, S.G. Cho, Y.I. Pae, S. Hayashi, J. Catal. 159 (1996) 170.
[38] J.R. Sohn, M.Y. Park, J. Ind. Eng. Chem. 4 (1998) 84.
[39] J.R. Sohn, D.H. Seo, S.H. Lee, J. Ind. Eng. Chem. 10 (2004) 309.
[40] J.R. Sohn, J.G. Kim, T.D. Kwon, E.H. Park, Langmuir 18 (2002) 1666.
[41] O. Saur, M. Bensitel, A.B.M. Saad, J.C. Lavalley, C.P. Tripp, B.A. Morrow, J. Catal. 99 (1986) 104.
[42] T. Yamaguchi, Appl. Catal. 61 (1990) 1.
[43] B.A. Morrow, R.A. McFarlane, M. Lion, J.C. Lavalley, J. Catal. 107 (1987) 232.
[44] J.R. Sohn, W.C. Park, Appl. Catal. A: Gen. 239 (2003) 269.
[45] R.V. Siriwardane, J.A. Poston Jr., E.P. Fisher, M.S. Shen, A.L. Miltz, Appl. Surf. Sci. 152 (1999) 219.
[46] J.R. Sohn, J. Ind. Eng. Chem. 10 (2004) 1.
[47] A. Satsuma, A. Hattori, K. Mizutani, A. Furuta, A. Miyamoto, T. Hattori, Y. Murakami, J. Phys. Chem. 92 (1988) 6052.
[48] J.R. Sohn, S.H. Lee, Appl. Catal. A: Gen. 266 (2004) 89.
[49] K. Arata, Adv. Catal. 37 (1990) 165.
[50] F.G.A. Olah, G.K.S. Prakash, J. Sommer, Science 206 (1979) 13.
[51] J.R. Sohn, E.H. Park, H.W. Kim, J. Ind. Eng. Chem. 5 (1999) 253.
[52] J.R. Sohn, S.G. Ryu, Langmuir 9 (1993) 126.
[53] T. Jin, T. Yamaguchi, K. Tananbe, J. Phys. Chem. 90 (1986) 4794.
[54] K. Tanabe, Solid Acids and Bases, Kodansha, Tokyo, 1970, p. 103.
[55] Y. Xia, W. Hua, Z. Gao, Appl. Catal. A: Gen. 185 (1999) 293.
[56] R.T. Sanderson, Chemical Bonds and Bond Energy, Academic Press, New York, 1976, p. 75.
[57] Z. Gao, Y. Xia, W. Hua, C. Miao, Topics Catal. 6 (1998) 101.